Improved self-consistency of the Reynolds stress tensor eigenspace perturbation for Uncertainty Quantification

Marcel Matha*[1] and Christian Morsbach[1]

German Aerospace Center (DLR), Linder Höhe, 51147 Cologne,

Germany

(*Electronic mail: marcel.matha@dlr.de.)

(Dated: 31 May 2023)

The limitations of turbulence closure models in the context of Reynolds-averaged Navier-Stokes (RANS) simulations play a significant part in contributing to the uncertainty of Computational Fluid Dynamics (CFD). Perturbing the spectral representation of the Reynolds stress tensor within physical limits is common practice in several commercial and open-source CFD solvers, in order to obtain estimates for the epistemic uncertainties of RANS turbulence models. Recent research revealed, that there is a need for moderating the amount of perturbed Reynolds stress tensor tensor to be considered due to upcoming stability issues of the solver. In this paper we point out that the consequent common implementation can lead to unintended states of the resulting perturbed Reynolds stress tensor. The combination of eigenvector perturbation and moderation factor may actually result in moderated eigenvalues, which are not linearly dependent on the originally unperturbed and fully perturbed eigenvalues anymore. Hence, the computational implementation is no longer in accordance with the conceptual idea of the Eigenspace Perturbation Framework. We verify the implementation of the conceptual description with respect to its self-consistency. Adequately representing the basic concept results in formulating a computational implementation to improve self-consistency of the Reynolds stress tensor perturbation.

Improved self-consistency of the Reynolds stress tensor eigenspace perturbation for UQ

I. INTRODUCTION

Industrial aerodynamic designs increasingly rely on numerical analysis based on flow simulations using Computational Fluid Dynamics (CFD) software. Such industrial applications usually feature turbulent flows. Due to its cost- and time-effective solution procedure, Reynolds-averaged Navier-Stokes (RANS) equations are an appropriate approach for design optimizations and virtual certification. Unfortunately, the Reynolds-averaged Navier-Stokes (RANS) equations are not closed and, hence, require the determination of the second-moment Reynolds stress tensor. In this context, the Reynolds stress tensor is approximated using turbulence models. These models make assumptions regarding the relationship between the Reynolds stresses and available mean flow quantities, such as the mean velocity gradients, which limit their applicability in terms of accuracy on the one hand. On the other hand, the assumptions made in the formulation of closure models inevitably lead to uncertainties as soon as their range of validity is left. The quantification of these model-form uncertainties for industrial purposes is a demanding task in general. Several approaches seek to account for these uncertainties at different modeling levels[1,2]. We focus on the Eigenspace Perturbation Framework (EPF)[3,4], which estimates the predictive uncertainty due to limitations in the turbulence model structure, namely its epistemic uncertainty. The EPF is purely physics-based and introduces a series of perturbations to the shape, alignment and size of the modeled Reynolds stress ellipsoid to estimate its uncertainty. Because of its straight forward implementation, the EPF has been used in diverse areas of application such as mechanical engineering[5], aerospace engineering[6–10], civil engineering[11,12], wind farm design[13,14], etc. The EPF is the foundation of recent confidence-based design under uncertainty approaches[15]. There have been studies showing the potential to optimize it using data driven machine learning approaches[16,17] and it has been applied for the virtual certification of aircraft designs[18,19]. The EPF has been integrated into several open and closed source flow solvers[20–23]. This range of applications emphasizes the importance of the EPF. Imperfections in the EPF can have a cascading ramification to all these applications and fields. There is need for Verification and Validation (V&V) for such novel methodologies. Validation focuses on the agreement of the computational simulation with physical reality[24], which has been done for the EPF in the aforementioned studies. On the other hand, verification focuses on the correctness of the programming and computational implementation of the conceptual model[25]. For the EPF, this verification would involve the theory behind the conceptual model and the compu-

tational implementation. The theoretical foundations of the Reynolds stress tensor perturbations have been analyzed in detail[26]. In this investigation, we focus on the computational implementation of the EPF, analyzing the consistency between the envisioned conceptual model and the actually implemented computational model.

In order to estimate the epistemic uncertainty for future design applications with respect to turbulence closure model, we review the current implementation of the framework in DLR's CFD solver suite *TRACE*. Especially, we focus on the motivation, implementation and effects of applying a moderation factor f, which serves to mitigate the amount of perturbation and aid numerical convergence of CFD solution[22,23] (in some publications f is called under-relaxation factor). The present investigation reveals a shortcoming when combining the eigenspace perturbation of the Reynolds stress tensor with the moderation factor, which has not yet been addressed in literature. On this basis, we formulate a way of improving self-consistency of the EPF and recovering its originally intended, physically meaningful idea in the present paper. Such self-consistency adherence is an essential component of the verification assessment stage of V&V [27] in order to ensure agreement between the conceptual and the computational model (numerical implementation), thus ensuring verification as outlined by AIAA CFD Committee[28].

The paper is structured as follows: Section II introduces the Reynolds stress tensor's eigenspace perturbation. We describe the fundamental motivation, the mathematical background and the deduced practical implementation of the EPF. In Section II A, we present the conceptual idea to apply an eigenspace decomposition of the anisotropy tensor. On this basis, the evident choice to perturb the eigenvalues and eigenvectors within physical limits is demonstrated from a practical engineering perspective in Section II B. Propagating these limiting states of turbulence enables a CFD practitioner to estimate the model-form uncertainty for certain Quantities of Interest (QoI) with respect to the underlying turbulence model. Finally, we point out an inconsistency in the prevailing computational implementation of the eigenspace perturbation in CFD solvers and suggest an alternative self-consistent formulation in Section II C. The uncertainty estimation for simulations of a turbulent boundary layer serve to demonstrate the envisioned benefits of the proposed consistent implementation of the EPF in Section II D. Section III summarizes the findings of the paper and assesses their significance for future applications.

II.   REYNOLDS STRESS TENSOR PERTURBATION TO ESTIMATE UNCERTAINTIES

A.   Reynolds stress anisotropy and visualization

The symmetric, positive semi-definite Reynolds stress tensor $\tau_{ij} = \overline{u_i' u_j'}$ needs to be determined by turbulence models in order to close the RANS equations. It can be decomposed into an anisotropy tensor a_{ij} and an isotropic part

$$\tau_{ij} = k \left(a_{ij} + \frac{2}{3} \delta_{ij} \right), \tag{1}$$

where the turbulent kinetic energy is defined as $k = \frac{1}{2} \tau_{kk}$ and summation over recurring indices within a product is implied. As the Reynolds stress tensor and its symmetric anisotropic part only contain real entries, they are diagonalizable. Thus, based on an eigenspace decomposition, the anisotropy tensor can be expressed as

$$a_{ij} = v_{in} \Lambda_{nl} v_{jl}. \tag{2}$$

The orthonormal eigenvectors form the Principal Coordinate System (PCS) and can be written as a matrix v_{in} while the traceless diagonal matrix Λ_{nl} contains the corresponding ordered eigenvalues λ_k with respect to $a_{ij}|_{\text{PCS}}$. Because of the definition of the anisotropy tensor in Eq. (1), Reynolds stress and anisotropy tensor share the same eigenvectors while the eigenvalues of the Reynolds stress tensor are $\rho_k = k(\lambda_k + 2/3)$. Consequently, the eigenvalues and the eigenvectors represent the shape and the orientation of the positive semi-definite (3,3)-tensor and can be visualized as an ellipsoid (see Fig. 1).

Generally, the anisotropy tensor describes and measures the deviation of the Reynolds stress tensor from the isotropic state, where its geometric ellipsoid representation forms a perfect sphere ($\rho_1 = \rho_2 = \rho_3$). The invariants of the anisotropy tensor

$$
\begin{aligned}
\text{I}_{\mathbf{a}} &= \text{tr}\,(\mathbf{a}) = 0 \\
\text{II}_{\mathbf{a}} &= -\frac{1}{2}\text{tr}\,(\mathbf{a}^2) = \lambda_1 \lambda_2 + \lambda_1 \lambda_3 + \lambda_2 \lambda_3 \\
\text{III}_{\mathbf{a}} &= \det(\mathbf{a}) = \lambda_1 \lambda_2 \lambda_3
\end{aligned}
\tag{3}
$$

can be used to visualize the tensor in a coordinate-system-invariant way, called the Anisotropy Invariant Map (AIM)[29], in Fig. 2.

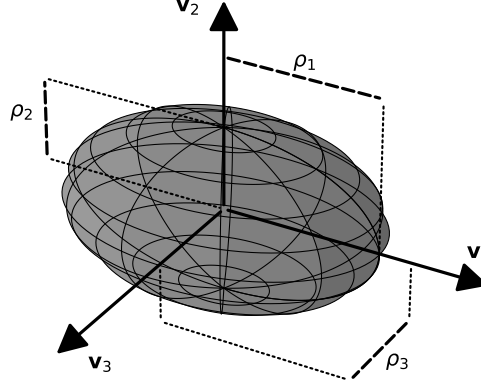Improved self-consistency of the Reynolds stress tensor eigenspace perturbation for UQ

FIG. 1. Representation of tensor as ellipsoid; eigenvalues ρ_k and eigenvectors v_k are highlighted.
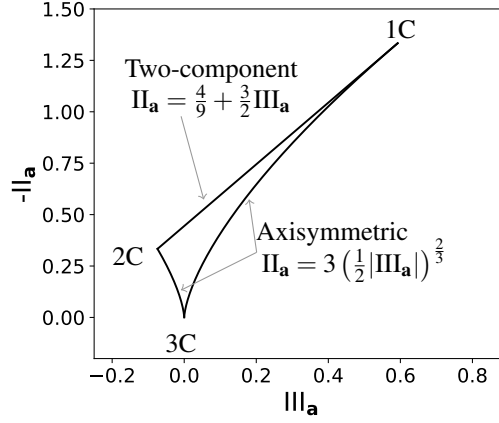

FIG. 2. AIM of the Reynolds stress tensor comparing second and third invariant of respective anisotropy tensor. The corners of the triangle (1C, 2C,3C) represent the componentiality of turbulence (see Table I).

Because of the physical realizability constraints of the Reynolds stress tensor[30]

$$\tau_{\alpha\alpha} \geq 0 \,, \quad \tau_{\alpha\alpha} \cdot \tau_{\beta\beta} \geq \tau_{\alpha\beta}^2 \,, \quad \det(\tau) \geq 0 \,, \quad \alpha, \beta = 1, 2, 3 \tag{4}$$

and the definition of the anisotropy tensor (see Eq. (1)), the entries of the anisotropy tensor are bounded in the following ranges:

$$a_{ij} \in \begin{cases} \left[-\frac{2}{3}, \frac{4}{3}\right] & \text{for } i = j \\ [-1, 1] & \text{for } i \neq j \end{cases} \,. \tag{5}$$

The eigenspace decomposition of the anisotropy tensor in combination with tensor diagonalization (see Eq. (2)) leads to the fact that any physically realizable Reynolds stress tensor can be mapped to exactly one respective anisotropy tensor in its canonical form $\Lambda_{ij} = \text{diag}(\lambda_1, \lambda_2, \lambda_3)$. Applying

TABLE I. Turbulence componentiality and limiting states of turbulence with respect to eigenvalues of the Reynolds stress tensor ρ_i and the anisotropy tensor λ_i.

States of turbulence	componentiality	eigenvalues	
	# $\rho_i \neq 0$ or # $\lambda_i \neq -\frac{2}{3}$	ρ_i	λ_i
One-component (1C)	1	$\rho_1 = 2k, \rho_2 = \rho_3 = 0$	$\lambda_1 = \frac{4}{3}, \lambda_2 = \lambda_3 = -\frac{2}{3}$
Two-component	2	$\rho_1 + \rho_2 = 2k, \rho_3 = 0$	$\lambda_1 + \lambda_2 = \frac{2}{3}, \lambda_3 = -\frac{2}{3}$
Two-component axisymmetric (2C)	2	$\rho_1 = \rho_2 = k, \rho_3 = 0$	$\lambda_1 = \lambda_2 = \frac{1}{3}, \lambda_3 = -\frac{2}{3}$
Three-component	3	$\rho_1 + \rho_2 + \rho_3 = 2k$	$\lambda_1 + \lambda_2 + \lambda_3 = 0$
Three-component isotropic (3C)	3	$\rho_1 = \rho_2 = \rho_3 = \frac{2}{3}k$	$\lambda_1 = \lambda_2 = \lambda_3 = 0$

Eq. (5) to Λ_{ij}, the ordered eigenvalues

$$\lambda_1 = \max_{\alpha} \left(a_{\alpha\alpha}|_{\text{PCS}} \right)$$
$$\lambda_2 = \max_{\beta \neq \alpha} \left(a_{\beta\beta}|_{\text{PCS}} \right) \tag{6}$$
$$\lambda_3 = -\lambda_1 - \lambda_2 = \min_{\gamma \neq \alpha, \beta} \left(a_{\gamma\gamma}|_{\text{PCS}} \right),$$

are bounded accordingly[31]:

$$\lambda_1 \geq \frac{3|\lambda_2| - \lambda_2}{2}, \lambda_1 \leq \frac{1}{3} - \lambda_2. \tag{7}$$

Turbulence componentiality[31] categorizes three fundamental states (one-, two- and three-component turbulence) based on the number of non-zero eigenvalues of the Reynolds stress tensor ρ_i (and respective anisotropy tensor eigenvalues λ_i), presented in Table I. Besides, axisymmetric turbulence is characterized by two eigenvalues being equal, while an isotropic state features three identical eigenvalues. The corners of the AIM in Fig. 2 can be classified as the (three-component) isotropic limit (3C), the two-component axisymmetric limit (2C) and the one-component limit (1C) (see also Table I). Moreover, due to the boundedness of the anisotropy tensor entries (and its eigenvalues, respectively), all physically plausible states of turbulence must lie within the area spanned by the corners of the triangle. Furthermore, due to the boundedness of the anisotropy tensor' eigenvalues, a barycentric triangle can be constructed based on the spectral theorem[32]. Consequently, every physically realizable state of the Reynolds stress tensor can be mapped onto

Improved self-consistency of the Reynolds stress tensor eigenspace perturbation for UQ

barycentric coordinates

$$\mathbf{x} = \frac{1}{2}\mathbf{x}_{1C}(\lambda_1 - \lambda_2) + \mathbf{x}_{2C}(\lambda_2 - \lambda_3) + \mathbf{x}_{3C}\left(\frac{3}{2}\lambda_3 + 1\right)$$

$$\mathbf{x} = \mathbf{Q}\boldsymbol{\lambda} \quad \text{with } \lambda_1 \geq \lambda_2 \geq \lambda_3 ,$$

(8)

where $\mathbf{Q}$ depends on the choice of corners of the barycentric triangle. Fig. 3 shows these three limiting states of the Reynolds stress tensor, defined by the corners of the triangle $(\mathbf{x}_{1C}, \mathbf{x}_{2C}, \mathbf{x}_{3C})$ representing the one-component, two-component axisymmetric and three-component (isotropic) turbulent state. A great benefit of the Anisotropy Barycentric Map (ABM) is the possibility to obtain a linear interpolation between two points with respect to their eigenvalues. The eigenspace perturbation exploits this property as well. Hence, we will come back to it later.

B. Perturbation of Eigenspace Representation

As the Reynolds stresses are expressed as functions of the mean flow quantities for turbulence modeling, we need to consider the nature of their relationship. A common example are the state-of-the-art Linear Eddy Viscosity Models (LEVM), which assume this relationship to be linear and introduce a turbulent (eddy) viscosity ν_t to approximate the Reynolds stress tensor in analogy to the viscous stresses

$$\tau_{ij} = -2\nu_t\left(S_{ij} - \frac{1}{3}\frac{\partial u_k}{\partial x_k}\delta_{ij}\right) + \frac{2}{3}k\delta_{ij} ,$$

(9)

where the strain-rate tensor is denoted as S_{ij}. In the past decades researchers have pointed out limitations of these LEVM for flow situations, which are not covered by the calibration cases[33–36]. The estimated relationship between Reynolds stresses and mean rate of strain results in the inability to account correctly for its anisotropy and consequently lead to a significant degree of epistemic uncertainty. In order to account for such epistemic uncertainties due to the model-form, the perturbation approach suggests to modify the eigenspace (eigenvalues and eigenvectors) of the Reynolds stress tensor within physically permissible limits[3,4]. The EPF of the Reynolds stress tensor implemented in *TRACE* creates a perturbed state of the Reynolds stress tensor defined as

$$\tau_{ij}^* = k\left(a_{ij}^* + \frac{2}{3}\delta_{ij}\right)$$

$$= k\left(v_{in}^*\Lambda_{nl}^*v_{jl}^* + \frac{2}{3}\delta_{ij}\right) ,$$

(10)

where a_{ij}^* is the perturbed anisotropy tensor, Λ_{nl}^* is the perturbed eigenvalue matrix and v_{in}^* is the perturbed eigenvector matrix. The turbulent kinetic k energy is left unchanged. In the follow-

ing sections, we will describe the mathematical and physical foundation of forming a perturbed eigenspace.

1. Eigenvalue perturbation

The eigenvalue perturbation utilizes the boundedness of the eigenvalues of the anisotropy tensor and their representation in terms of barycentric coordinates, as described in Section II A. As the representation of the anisotropy tensor within the ABM enables linear interpolation between a starting point $\mathbf{x}$ and a target point $\mathbf{x}_{(t)}$, the perturbation methods creates a modified location $\mathbf{x}^*$, according to

$$\mathbf{x}^* = \mathbf{x} + \Delta_B \left(\mathbf{x}_{(t)} - \mathbf{x} \right) , \tag{11}$$

with the relative distance $\Delta_B \in [0,1]$ controlling the magnitude of eigenvalue perturbation as illustrated in Fig. 3. The starting point $\mathbf{x}$ is usually determined in the RANS simulation iteration via the relationship for the Reynolds stresses determined by the turbulence model, e.g. the Boussinesq assumption for LEVM (see Eq. (9)). Due to their distinctive significance, the limiting states of turbulence at the corners act typically as the target point $\mathbf{x}_{(t)} \in \{\mathbf{x}_{1C}, \mathbf{x}_{2C}, \mathbf{x}_{3C}\}$. Subsequently, the perturbed eigenvalues λ_i^* can be remapped by the inverse of $\mathbf{Q}$

$$\boldsymbol{\lambda}^* = \mathbf{Q}^{-1} \mathbf{x}^* . \tag{12}$$

2. Eigenvector perturbation

In contrast to the eigenvalues, there are no physical bounds for the orientation of the eigenvectors of the Reynolds stress tensor and there is no upper limit for the turbulent kinetic energy. Thus, the fundamental idea of perturbing the eigenvectors is to create bounding states for the production P_k of turbulent kinetic energy k in transport equation based LEVM. Hereby, the budget of turbulent kinetic energy is indirectly manipulated. The turbulent production term is defined as the Frobenius inner product of the Reynolds stress and the strain-rate tensor. Since both are positive semi-definite, the bounds of the Frobenius inner product can be written in terms of their eigenvalues ρ_i and σ_i arranged in decreasing order[37]:

$$P_k = -\tau_{ij} \frac{\partial u_i}{\partial x_j} = -\tau_{ij} \cdot S_{ij} = -\langle \boldsymbol{\tau}, \mathbf{S} \rangle_F = -\mathrm{tr}\left(\boldsymbol{\tau} \mathbf{S} \right)$$

$$\in \left[\rho_1 \sigma_3 + \rho_2 \sigma_2 + \rho_3 \sigma_1, \rho_1 \sigma_1 + \rho_2 \sigma_2 + \rho_3 \sigma_3 \right] . \tag{13}$$
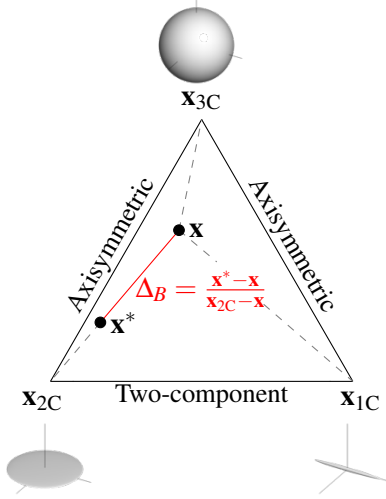
8

FIG. 3. ABM representing the eigenvalues of the anisotropy tensor and its effect on the shape of the Reynolds stress tensor ellipsoid. The eigenvalue perturbation towards the two-component limiting state of turbulence is shown schematically.

Since the Reynolds stress and the strain rate tensor share the same eigenvectors in LEVM (see Eq. (9)), the lower bound of the turbulent production term can be obtained by commuting the first and third eigenvector of the Reynolds stress tensor, whereas maximum turbulent production is obtained by not changing the eigenvectors of the Reynolds stress tensor:

$$
\begin{aligned}
\mathbf{v}_{\text{max}} &= \begin{pmatrix} \mathbf{v}_{1_{\mathbf{S}}} & \mathbf{v}_{2_{\mathbf{S}}} & \mathbf{v}_{3_{\mathbf{S}}} \end{pmatrix} \rightarrow P_{k_{\text{max}}} \\
\mathbf{v}_{\text{min}} &= \begin{pmatrix} \mathbf{v}_{3_{\mathbf{S}}} & \mathbf{v}_{2_{\mathbf{S}}} & \mathbf{v}_{1_{\mathbf{S}}} \end{pmatrix} \rightarrow P_{k_{\text{min}}} \, .
\end{aligned}
\tag{14}
$$

Note: Permuting of the eigenvectors of the Reynolds stress is equivalent to changing the order of the respective eigenvalues. Both change the alignment of the Reynolds stress ellipsoid with the principle axes of the strain-rate tensor.

3. Implications for CFD practitioners

The eigenspace perturbation can be divided into eigenvalue and eigenvector modifications of the Reynolds stress tensor. For practical application purposes each eigenvalue perturbation towards one of the limiting states of turbulence can be combined with minimization or maximization of the turbulent production term (eigenvector perturbation). In summary, the model-form uncertainty of LEVM can be estimated by 6 additional CFD simulations if $\Delta_B < 1$ and only 5 perturbed simu-

lations if $\Delta_B = 1$ is chosen. This is because the Reynolds stress ellipsoid is a perfect sphere when targeting for the 3C turbulence state with $\Delta_B = 1$ (see Fig. 3), making an eigenvector perturbation obsolete. As the amount of considered turbulence model uncertainty scales with the relative perturbation strength Δ_B, aiming for the corners of the barycentric triangle (applying $\Delta_B = 1$) is common practice in order to obtain a worst case estimate corresponding to the most conservative uncertainty bounds on QoI [3,4,22,23]. The analysis of additional CFD simulations, propagating the effect of perturbed Reynolds stress tensor, enables a CFD practitioner to quantify the derived effect of the turbulence model perturbation on certain QoI, e.g. the pressure field.

C. Self-consistent formulation of perturbation

The emergence of some shortcomings of the eigenspace perturbation of the Reynolds stress tensor is highlighted in this section. This forms the foundation of rethinking of the computational formulation the EPF. The present paper suggests an appropriate way of formulating the EPF, ensuring control over numerical stability while preserving the conceptual model of perturbing the eigenspace of the Reynolds stress tensor.

1. Need for moderating the perturbation strength

The need for moderating the effect of Reynolds stress tensor perturbation emerges, when the Reynolds stress tensor perturbation seeks to decrease the turbulent kinetic energy budget ($P_{k_{\min}}$ and/or 3C). These perturbations featuring overly reduced turbulent viscosity can lead to numerical convergence issues for example when simulating separated flows. To ensure convergence while still perturbing as much as required, there is a need to moderate the effect of Reynolds stress tensor perturbation. Recent publications introduce a moderation factor f to enable the CFD-solver to achieve fully converged, steady-state RANS results[22,23]. Consequently, the propagated perturbed Reynolds stress tensor (entering the update of the viscous fluxes and the turbulent production term) can be expressed as

$$\tau^*_{ij_f} = \tau_{ij} + f \left[\tau^*_{ij} - \tau_{ij} \right], \tag{15}$$

where $f \in [0,1]$ is the introduced moderation factor, adjusting the total amount of perturbed anisotropy tensor to be considered. Note: The effect of applying the moderation factor is identical to a reduction of Δ_B in Eq. (11) in case of pure eigenvalue perturbation[23].
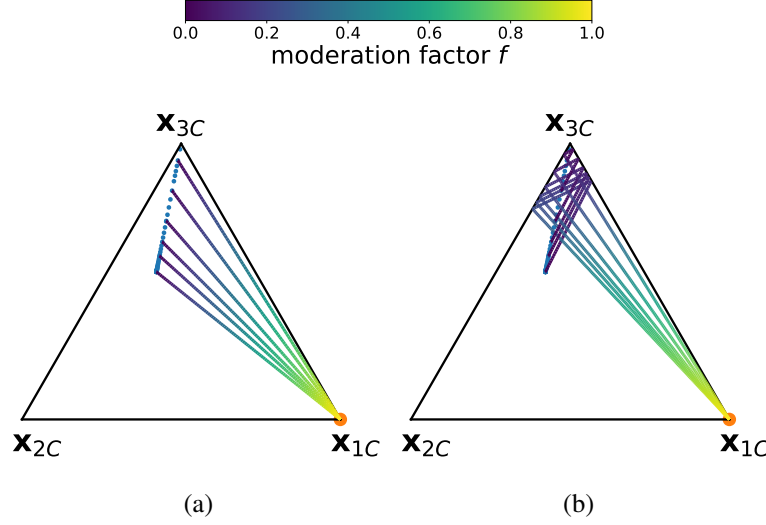
FIG. 4. Comparison of perturbation trajectory for RANS channel flow data at $Re_\tau = 1000$ (blue dots) in barycentric coordinates. The trajectories for selected RANS data points (τ_{ij}) are created by increasing $f = 0...1$ with and without eigenvector perturbation targeting the one-component limiting state of turbulence $\tau_{ij}^* = \tau_{ij_{1C}}$ (orange dot). (a) Without eigenvector modification (aiming for $P_{k_{max}}$). (b) Perturbation including eigenvector modification (aiming for $P_{k_{min}}$).

2. Inconsistency when combining eigenspace perturbation and moderation factor

Unfortunately, the unperturbed Reynolds stress tensor τ_{ij} and the perturbed one τ_{ij}^* do not necessarily share the same eigenvectors. When eigenvector perturbation is applied, the resulting moderated Reynolds stress tensor $\tau_{ij_f}^*$ shows unintended behaviour with respect to its projection onto barycentric coordinates. Fig. 4 presents the perturbation trajectory when increasing f from 0 to 1 for selected RANS data points inside the AIM towards the one-component limiting state of turbulence. The moderated Reynolds stress tensor is calculated based on Eq. (15) with $\tau_{ij}^* = \tau_{ij_{1C}}$, while $\tau_{ij_{1C}}$ is a function of $\Lambda_{ij_{1C}}^*$, $\mathbf{v}_i^*$ and k_{RANS}. Each location along the perturbation trajectory results from determining the respective moderated anisotropy tensor and its barycentric coordinates related to its eigenvalues. The perturbation trajectory when τ_{ij}^* and τ_{ij} share identical eigenvectors shows the expected linear interpolation between the respective coordinates. However, when applying eigenvector perturbation (first and last column of v_{jl}^* are commuted) the resulting intermediate paths do not represent the most direct connection between starting and target point. Instead, the perturbation trajectories in Fig. 4b point towards axisymmetric expansion (line between $\mathbf{x}_{3C}$ and $\mathbf{x}_{1C}$) first, head towards axisymmetric contraction (line between $\mathbf{x}_{3C}$ and $\mathbf{x}_{2C}$) subsequently and

11

target the one-component limit of turbulence finally.

The mathematical explanation for this observation, when combining eigenvalue and eigenvector perturbation while moderating their effects by a factor according to Eq. (15) is given thereupon. Thus, the prerequisites for the accomplishment of linear interpolation properties in terms of barycentric coordinates, when adding two tensors $\mathbf{X}$ and $\mathbf{Y}$, are addressed. Assuming $\mathbf{X}$ and $\mathbf{Y}$ are positive semi-definite (as the Reynolds stress tensor), then these tensors are realizable[30] and their projection onto barycentric coordinates has to lie within the barycentric triangle[32], following the reasons mentioned above (see Section II A). If $\mathbf{X}$ and $\mathbf{Y}$ share identical eigenvectors (commuting matrices), their sum $\mathbf{X}+\mathbf{Y}$ will feature the same eigenvectors and its eigenvalues are the sum of the individual eigenvalues of $\mathbf{X}$ and $\mathbf{Y}$ consequently (see Appendix A). Moreover, if $\mathbf{X}$ and $\mathbf{Y}$ are positive semi-definite, their sum $\mathbf{X}+\mathbf{Y}$ will be positive semi-definite as well (see Appendix B). This implies, that the sum of two realizable Reynolds stress tensors will fulfill realizability constraints and will be located inside the ABM accordingly.

The line of argument mentioned above is also true for the summation of two scaled tensors

$$\mathbf{Z} = \mathbf{X} + f\left[\mathbf{Y} - \mathbf{X}\right] = (1 - f)\mathbf{X} + f\mathbf{Y}\,, \tag{16}$$

as multiplying a tensor by a scalar does not affect the eigenvectors and modifies the eigenvalues linearly. The individual scaling of the tensors is chosen, such that the first invariant of $\mathbf{Z}$ ($\mathrm{tr}\,(\mathbf{Z})$) remains identical to $\mathbf{X}$ and $\mathbf{Y}$ ($\mathrm{tr}\,(\mathbf{X}) = \mathrm{tr}\,(\mathbf{Y}) = \mathrm{tr}\,(\mathbf{Z})$). Keeping in mind, that $\mathbf{X}$ and $\mathbf{Y}$ represent Reynolds stress tensors, this means, that the turbulent kinetic energy remains constant. This is achieved by choosing $f \in [0,1]$. Due to the affine transformation, the barycentric coordinates of the anisotropic part of $\mathbf{Z}$ are determined by $\mathbf{x_Z} = (1 - f)\,\mathbf{x_X} + f\mathbf{x_Y}$, when $\mathbf{x_X}$ and $\mathbf{x_Y}$ are the initial states of the tensors $\mathbf{X}$ and $\mathbf{Y}$ in barycentric coordinates (see Appendix C). Finally, if f is increased incrementally from 0 to 1, the resulting states $\mathbf{x_Z}$ will end up forming a straight line connecting $\mathbf{x_X}$ and $\mathbf{x_Y}$, as illustrated in Fig. 5 and especially in Fig. 5a. For reference, Fig. 5b and Fig. 5c show the result of linear interpolation in terms of barycentric coordinates in the classical AIM and the alternative Anisotropy Invariant Map[38].

However, the summation of commuting matrices is the exception. Adding up two arbitrary, positive semi-definite matrices, eigenvector orientation is not preserved and the resulting eigenvalues are not just the sum of the original eigenvalues. As a consequence, their transformation into barycentric coordinates is not located along the shortest possible path connecting the representation of the anisotropy of the original tensors, as shown in Fig. 6. Analyzing the orientation
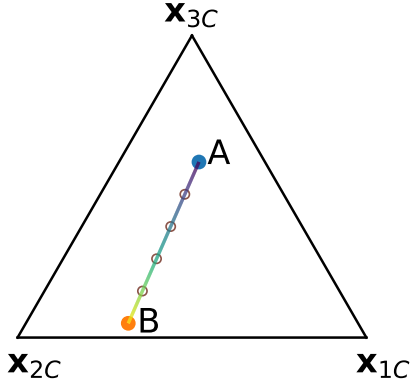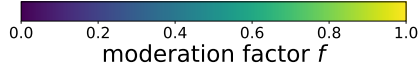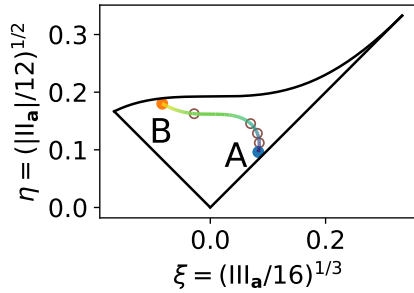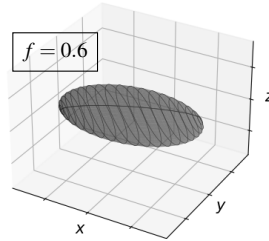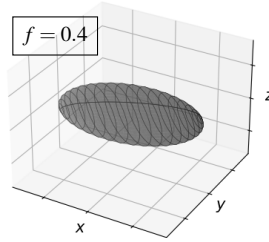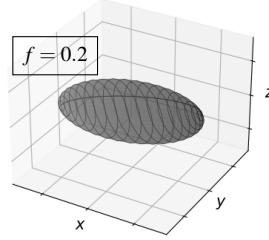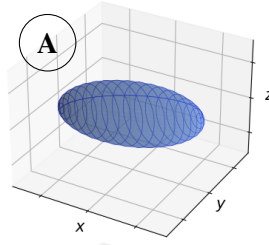
(a) Representation in ABM[32]
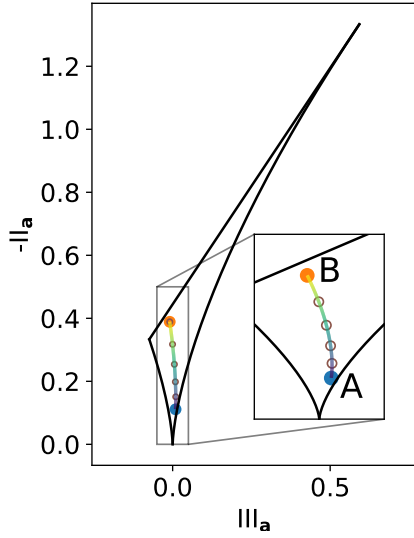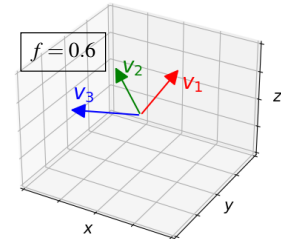
(b) Representation in AIM[29]

(c) Representation in alternative Anisotropy Invariant Map[38]
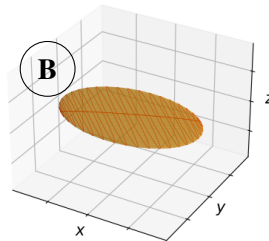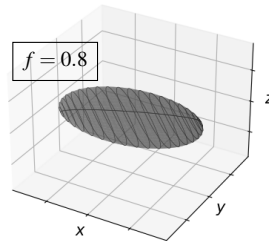
(d) Reynolds stress tensor ellipsoid
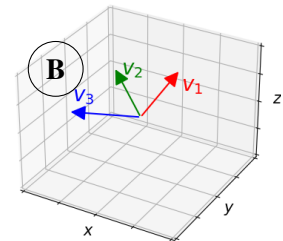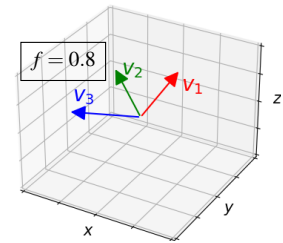
(e) Eigenvectors of Reynolds stress tensor

FIG. 5. Transition from tensor **A** to **B** (defined in Appendix D) featuring identical eigenvectors by increasing $f = 0...1$ (see Eq. (16)). The intermediate brown-colored states in (a), (b) and (c) correspond to the states with $f \in [0.2, 0.4, 0.6, 0.8]$ in (d) and (e).
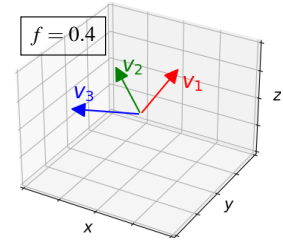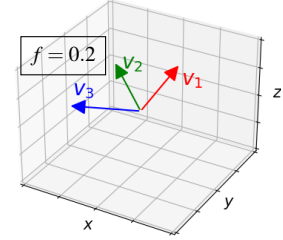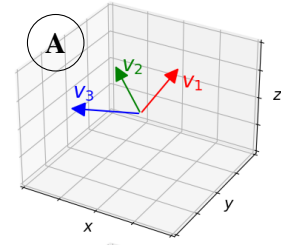
(a) Representation in ABM[32]

(b) Representation in AIM[29]

(c) Representation in alternative Anisotropy Invariant Map[38]

(d) Reynolds stress tensor ellipsoid

(e) Eigenvectors of Reynolds stress tensor
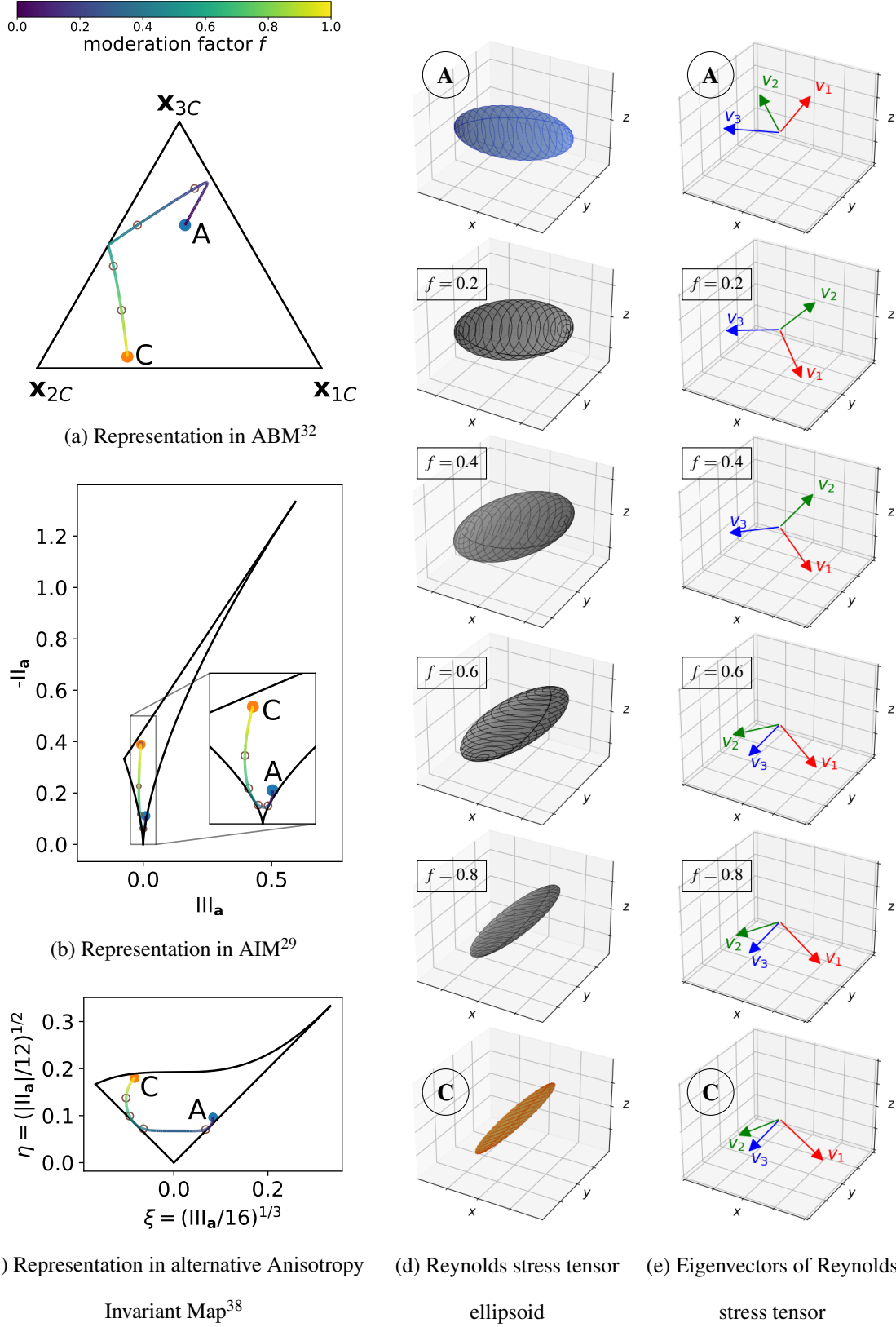
FIG. 6. Transition from tensor **A** to **C** (defined in Appendix D) featuring different eigenvector by increasing $f = 0...1$ (see Eq. (16)). The intermediate brown-colored states in (a), (b) and (c) correspond to the states with $f \in [0.2, 0.4, 0.6, 0.8]$ in (d) and (e).

of the PCS of each tensor in Fig. 6d and Fig. 6e reveals the transformation of eigenspace. The representation in barycentric coordinates shows a perturbation trajectory which connects starting and target point via the sides of the triangle (see Fig. 6a). Hence, the introduction of a moderation factor violates the original intent of the EPF and, in addition to that, affects the plausibility of recent data-driven machine learning approaches[16,23], relying on the interpolation property with respect to barycentric coordinates. Moreover, the bounds of the Frobenius inner matrix product (see Eq. (14)) can only be achieved, if the matrices share the same eigenvectors. When applying Reynolds stress eigenvector perturbation in combination with a moderation factor, the resulting turbulent production indeed yields a value within the interval of the inner product defined in Section II B 2, but does not reach the theoretical limits as the perturbed Reynolds stress tensor features some different eigenvectors compared to the strain-rate tensor.

To sum up, the concept of the EPF, which is perturbing the eigenvalues of the Reynolds stress tensor linearly between the initial state and a certain limiting state of turbulence, cannot be guaranteed if a moderation factor is introduced as in current implementations. Applying this moderation factor in combination with eigenvector perturbations results in an conceptually unintended state of the anisotropy tensor on the one hand. On the other hand, the intended minimization and maximization of the turbulent production term is no longer guaranteed.

3. *Proposed approach to improve self-consistency*

In order to resolve the issues described in Section II C 2 the implementation of the EPF needs to be changed. A first step is the removal of the entire idea of applying a moderation factor to adjust the amount of perturbed Reynolds stress tensor according to Eq. (15). As a consequence, Δ_B in Eq. (11), which controls the amount of perturbation towards the respective limiting state of turbulence, has to be adjusted, in order to retain converged RANS simulations (see Section II C 1). This is in contrast to the the common practice of choosing $\Delta_B = 1.0$, arguing that there is no physical reason to restrict this value without the usage of data-driven methods or expert knowledge on the flow configuration. In other words, the perturbed Reynolds stress tensor, entering the update of the viscous fluxes and the turbulent production term, in the proposed self-consistent implementation is equal to Eq. (10). Nevertheless, the fundamental idea of the individual perturbation of eigenvalues and eigenvectors, introduced in Section II B 1, remains the same. Hereby, the entire EPF in order to quantify the structural uncertainties of turbulence models is formulated in a verified,

Improved self-consistency of the Reynolds stress tensor eigenspace perturbation for UQ

physics-constrained and self-consistent manner. Its implementation in *TRACE* can be subdivided in several steps within each pseudo-time step of steady RANS:

1. Calculate Reynolds stress tensor based on Boussinesq approximation in Eq. (9)

2. Determine respective anisotropy tensor (see Eq. (1)).

3. Decompose the anisotropy tensor in its eigenvalues and eigenvectors (see Eq. (2)).

4. Compute the barycentric coordinates based on eigenvalues of the anisotropy tensor (see Eq. (8)).

5. Perturb the barycentric coordinates of the anisotropy tensor within physical realizable limits by chosen Δ_B (see Eq. (11))

6. Determine perturbed eigenvalues of the anisotropy tensor with respect to the perturbed barycentric coordinates (see Eq. (12))

7. Perturb the eigenvectors of anisotropy/Reynolds stress tensor if turbulent production term should be minimized (see Eq. (14)).

8. Reconstruct the perturbed Reynolds stress tensor according to Eq. (10)

9. Update the viscous fluxes using the reconstructed perturbed Reynolds stress tensor

10. Update the turbulence production term using the reconstructed perturbed Reynolds stress tensor explicitly

Note: Different types and magnitudes of the perturbations (1C, 2C or 3C; $P_{k_{\min}}$ or $P_{k_{\max}}$; chosen Δ_B and/or f) result in different solutions of the RANS equations from a mathematical point of view regardless of the EPF formulation (non-consistent or consistent). However, not every mathematical solution represents a physically meaningful solution (e.g. a solution giving laminar flow in a clearly turbulent domain, or unsteady flow in steady state conditions). Hence, the EPF requires certain expert knowledge and engineering practice to determine the appropriate amount of perturbation magnitude (Δ_B in the consistent formulation) leading to meaningful, converged RANS solutions.
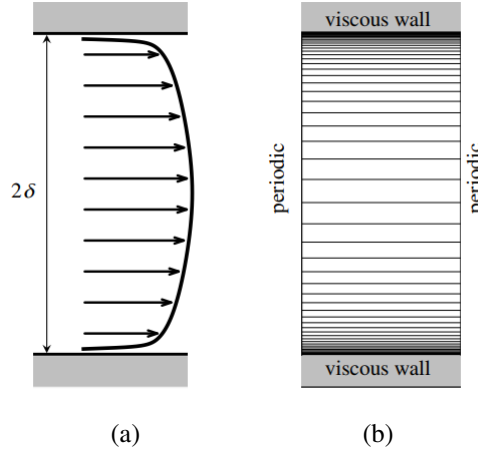
(a)   (b)

FIG. 7. Turbulent channel flow simulation. (a) Schematic sketch of a fully developed turbulent boundary layer. (b) Mesh (every fourth line shown) and boundary conditions; symmetry is enforced in spanwise direction.

D. Application to plane turbulent channel flow

The uncertainty estimates based on the non-consistent and self-consistent eigenspace perturbation are compared when applied to a canonical turbulent channel flow at $Re_\tau = 1000$. The channel flow is homogeneous in streamwise and spanwise direction. A constant streamwise pressure gradient $\partial p/\partial x$ is applied to balance the skin friction at the walls. The configuration for simulating this wall-bounded flow is sketched in Fig. 7. The mesh has a low-Reynolds resolution ($y^+ \leq 1$) at the solid walls with 100 cells up to the symmetry line in wall-normal direction. The two-equation Menter SST k-ω turbulence model[39], which belongs to the group of LEVM, is considered as the baseline model for the present simulations. The discrepancies with respect to barycentric coordinates of the RANS turbulence model when compared with available Direct Numerical Simulation (DNS) data[40] are moderate in the channel center and start to increase close to the wall due to the strong anisotropy of turbulence (see Fig. 8). Due to the fact, that the turbulence model relies on the Boussinesq assumption Eq. (9) and that a velocity gradient in spanwise direction is missing, the Reynolds stress tensor has at least one zero eigenvalue. Hence, the resulting barycentric coordinates are known to be the plane-strain line in the ABM.

The turbulence model-form uncertainty is quantified applying the EPF. In order to demonstrate the implications of using the proposed consistent formulation a relative perturbation strength of $\Delta = 0.5$ is used for the consistent formulation, while $\Delta = 1.0$ is used for the non-consistent formu-
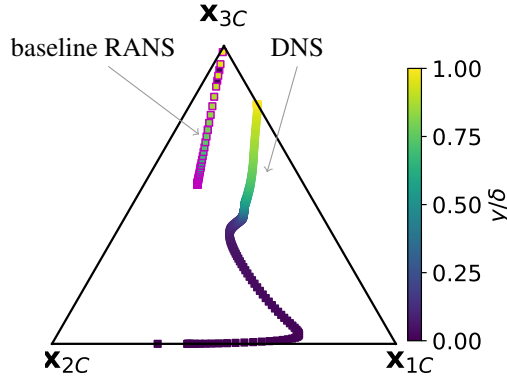
FIG. 8. Barycentric coordinates of DNS data and RANS simulation using baseline turbulence model MenterSST k-ω. Data points are colored according to their distance from the wall.

lation. Consequently, a factor of $f = 0.5$ is applied for the non-consistent formulation to moderate the strength for eigenvalues and eigenvector perturbation and to obtain comparable results to the consistent formulation. The streamwise pressure gradient, which was adjusted for the baseline simulation to match the Reynolds number, remains constant throughout the perturbed simulations. This is comparable to the procedure of Emory et al. for a similar test case[3]. The comparison of the uncertainty estimated by the EPF for the streamwise velocity profile of the boundary layer is presented in Fig. 9. The simulations featuring eigenvector perturbation are indicated by $P_{k_{\min}}$ (leading to minimized turbulent production), while no eigenvector permutation is applied for $P_{k_{\max}}$ (see Eq. (14)). Overall, the uncertainty estimate (grey shaded area) of the boundary layer profile are identical for both formulations. On the one hand, this is because the simulations without any eigenvector perturbation are mathematically equivalent, leading to identical results for QoI. On the other hand, applying eigenvector permutation for the channel flow results in laminarization of the boundary layer. Hence, the laminar velocity profile driven by the selected constant streamwise pressure gradient bounds the uncertainty estimation, regardless of EPF formulation or target barycentric coordinate $\mathbf{x}_{(t)}$. Overall, the uncertainty intervals are smaller for previous investigations of the channel flow by Emory et al.[3]. To the authors' knowledge and experience, this is because of the fact, that Emory et al. do not explicitly update the turbulent production term based on the perturbed Reynolds stresses. Additionally, as the perturbations for both formulations are uniform throughout the computational domain, it is expected, that by applying an appropriate amount of perturbation strength (e.g. locally varying perturbations with the help of machine learning) the uncertainty estimates would be more adequate.
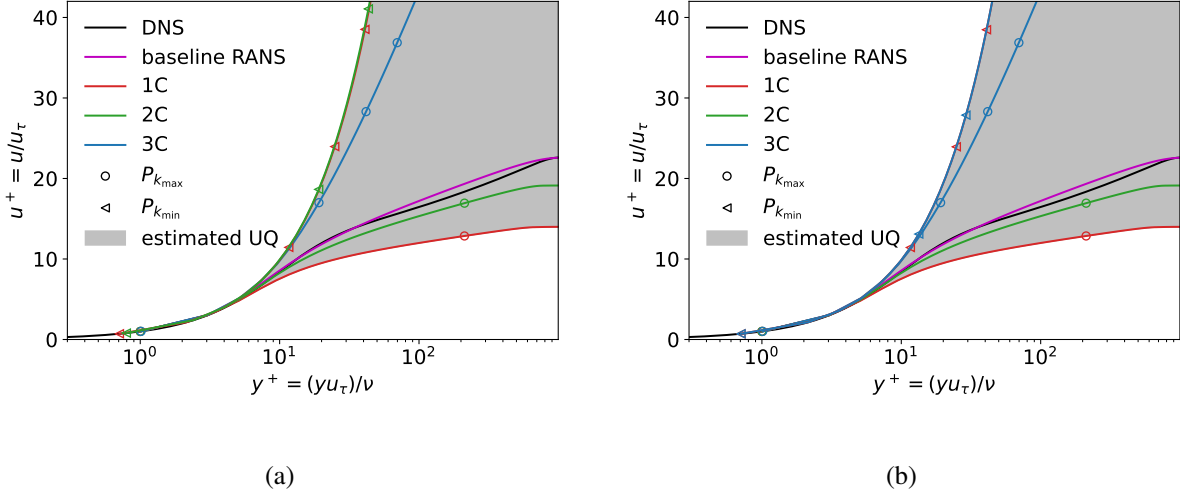
FIG. 9. Comparison of resulting uncertainty bounds for streamwise velocity profile of turbulent channel flow simulation derived by EPF. (a) Application of non-consistent formulation of EPF using $\Delta_B = 1.0$ and $f = 0.5$. (b) Application of consistent formulation of EPF using $\Delta_B = 0.5$.

In terms of conceptual model verification, the proposed self-consistent formulation guarantees to maintain agreement between the theoretical idea of the EPF and the simulation results, which are shown in Fig. 10. The final perturbed states of the Reynolds stress tensor anisotropy for simulations aiming at $P_{k_{\max}}$, show the expected, identical perturbed anisotropic states for both EPF formulations. Fig. 10a reveals the initial motivation for scrutinizing the consistency of the formulation using a moderation factor in combination with eigenvector perturbation as the RANS solution points for the turbulent boundary layer do not show the intended behaviour for $P_{k_{\min}}$. If a CFD practitioner runs a perturbed RANS simulation aiming for one of the corners of the barycentric triangle, it is expected that the resulting anisotropic states show respective shifts towards that limiting state of turbulence. The boundary layer solution points of $(1C, P_{k_{\min}})$ and $(2C, P_{k_{\min}})$ are located at some unintended states inside the barycentric triangle in Fig. 10a due to summation of two non-commuting tensors. In contrast, the respective simulations using the consistent formulation produces anisotropic states of the Reynolds stress tensor, which are entirely perturbed towards one of the corners of the triangle (keeping in mind, that the unperturbed Reynolds stress tensor is represented by the plane-strain line as in Fig. 8).

Note: The self-consistent formulation of the EPF framework, presented in Section II C 3, enables the user to additionally perform the perturbed RANS simulation aiming for $(3C, P_{k_{\min}})$, which was obsolete in the non-consistent formulation using $\Delta_B = 1.0$.
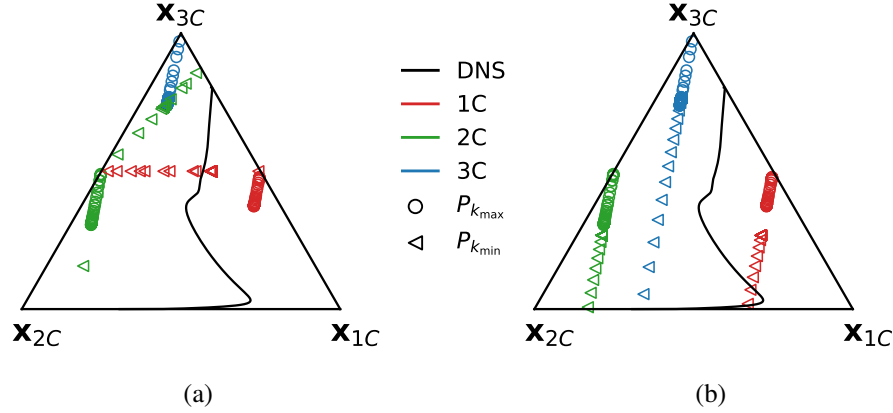
FIG. 10. Comparison of resulting barycentric coordinates of the perturbed Reynolds stress tensors for turbulent boundary layer profiles in Fig. 9. (a) Application of non-consistent formulation of EPF using $\Delta_B = 1.0$ and $f = 0.5$. (b) Application of consistent formulation of EPF using $\Delta_B = 0.5$.

III. CONCLUSION & OUTLOOK

The EPF, that creates perturbed states of the Reynolds stress tensor in order to quantify the structural uncertainties of RANS turbulence models, is described in detail, presenting its underlying idea and discussing its practical implementation and usage. The present work highlights one shortcoming in the commonly proposed implementation of this framework. Due to numerical convergence issues, researchers have suggested to weaken the effect of perturbed Reynolds stress by introducing a moderation factor in previous publications. The assessment of the common computational implementation reveals, that the basic concept of the EPF is not correctly represented in that case. The introduction of a separate moderation factor may cause unintended behaviour and violate EPF's self-consistency. Therefore, the present paper presents a self-consistent way of formulating the Reynolds stress tensor perturbation framework, as the significance of reasonable physics-constrained Uncertainty Quantification methodologies is indisputable. This formulation has recently been implemented in DLR's CFD solver suite *TRACE*. The analysis of the results based on the proposed eigenspace perturbation formulation when applied to turbulent channel flow verifies its benefits with respect to the interpretability of the uncertainty estimates. In the near future the framework will be applied to quantify the uncertainties for more complex flows for which the differences between the non-consistent and the self-consistent formulation are expected to be greater for QoI. Moreover, ongoing research focusing on determining the Reynolds stress

Improved self-consistency of the Reynolds stress tensor eigenspace perturbation for UQ

tensor perturbation by the use of data-driven machine learning practises will benefit from verified self-consistent implementation of the framework as well.

ACKNOWLEDGMENTS

DATA AVAILABILITY STATEMENT

The data that support the findings of this study are available from the corresponding author upon reasonable request.

Appendix A: Properties of the sum of two tensors featuring identical eigenvectors in terms of eigenspace

Let ϕ_i be the eigenvalues of tensor $\mathbf{X}$ and ψ_i be the eigenvalues of tensor $\mathbf{Y}$. Both tensors share the same eigenvectors w_i. Therefore, we know, that the relationships

$$
\begin{aligned}
\mathbf{X}\mathbf{w}_i &= \phi_i \mathrm{w}_i \quad i = 1,2,3 \\
\mathbf{Y}\mathbf{w}_i &= \psi_i \mathrm{w}_i \quad i = 1,2,3
\end{aligned}
\tag{A1}
$$

are satisfied. The summation of $\mathbf{X}$ and $\mathbf{Y}$ leads to:

$$
\begin{aligned}
(\mathbf{X}+\mathbf{Y})\mathbf{w}_i &= \mathbf{X}\mathbf{w}_i + \mathbf{Y}\mathbf{w}_i \quad i = 1,2,3 \\
&= \phi_i \mathbf{w}_i + \psi_i \mathbf{w}_i \text{ (cf. Eq. (A1))} \\
&= (\phi_i + \psi_i)\mathbf{w}_i
\end{aligned}
\tag{A2}
$$

Consequently, the resulting sum features identical eigenvectors as well and its eigenvalues are the sum of the individual eigenvalues.

Appendix B: Transferability of definiteness related to the sum of two positive semi-definite tensors

Tensor $\mathbf{X}$ and tensor $\mathbf{Y}$ are positive semi-definite, which means

$$\forall \mathbf{u} \in \mathbb{R}^n, \ \mathbf{u}^T \mathbf{X} \mathbf{u} \geq 0, \ \mathbf{u}^T \mathbf{Y} \mathbf{u} \geq 0 \,. \tag{B1}$$

The sum of $\mathbf{X}$ and $\mathbf{Y}$ can be distributed based on the laws of tensor multiplication

$$\forall \mathbf{u} \in \mathbb{R}^n, \mathbf{u}^T (\mathbf{X} + \mathbf{Y}) \mathbf{u} = \mathbf{u}^T \mathbf{X} \mathbf{u} + \mathbf{u}^T \mathbf{Y} \mathbf{u} \geq 0 \tag{B2}$$

Consequently, the sum of two positive semi-definite tensors is positive semi-definite as well.

Appendix C: Interpolation properties of two scaled tensor with respect its location in barycentric coordinates

Let $\phi_1 \geq \phi_2 \geq \phi_3$ be the eigenvalues of the anisotropic part of the (3,3)-tensor $\mathbf{X}$ and $\psi_1 \geq \psi_2 \geq \psi_3$ be the eigenvalues of the anisotropic part of the (3,3)-tensor $\mathbf{Y}$. The eigenvalues of the summation of the scaled tensors

$$\mathbf{Z} = (1 - f)\mathbf{X} + f\mathbf{Y} \tag{C1}$$

Improved self-consistency of the Reynolds stress tensor eigenspace perturbation for UQ

are $\sigma_i = (1 - f)\phi_i + f\psi_i$. The barycentric coordinates are

$$
\mathbf{x_Z} = \mathbf{x}_{1C}\frac{1}{2}[\sigma_1 - \sigma_2] + \mathbf{x}_{2C}[\sigma_2 - \sigma_3] + \mathbf{x}_{3C}\left[\frac{3}{2}\sigma_3 + 1\right] \tag{C2}
$$

$$
\begin{aligned}
= \mathbf{x}_{1C}\frac{1}{2}&[((1-f)\phi_1 + f\psi_1) - ((1-f)\phi_2 + f\psi_2)] \\
&+ \mathbf{x}_{2C}[((1-f)\phi_2 + f\psi_2) - ((1-f)\phi_3 + f\psi_3)] \\
&+ \mathbf{x}_{3C}\left[\frac{3}{2}((1-f)\phi_3 + f\psi_3) + 1\right]
\end{aligned} \tag{C3}
$$

$$
\begin{aligned}
= \mathbf{x}_{1C}\frac{1}{2}&[((1-f)\phi_1 + f\psi_1) - ((1-f)\phi_2 + f\psi_2)] \\
&+ \mathbf{x}_{2C}[((1-f)\phi_2 + f\psi_2) - ((1-f)\phi_3 + f\psi_3)] \\
&+ \mathbf{x}_{3C}\left[\frac{3}{2}((1-f)\phi_3 + f\psi_3) + 1 - f + f\right]
\end{aligned} \tag{C4}
$$

$$
\begin{aligned}
= \mathbf{x}_{1C}\frac{1}{2}&[(1-f)(\phi_1 - \phi_2)] \\
&+ \mathbf{x}_{2C}[(1-f)(\phi_2 - \phi_3)] \\
&+ \mathbf{x}_{3C}\left[\frac{3}{2}(1-f)(\phi_3 + 1)\right] \\
&+ \mathbf{x}_{1C}\frac{1}{2}[f(\psi_1 - \psi_2)] \\
&+ \mathbf{x}_{2C}[f(\psi_2 - \psi_3)] \\
&+ \mathbf{x}_{3C}\left[\frac{3}{2}f(\psi_3 + 1)\right]
\end{aligned} \tag{C5}
$$

$$
= (1 - f)\mathbf{x_X} + f\mathbf{x_Y} \tag{C6}
$$

Consequently, the projection onto barycentric coordinates preserves the ability to interpolate linearly between two initial states in the ABM.

Appendix D: Example tensors used in this paper

The positive semi-definite tensor $\mathbf{A}$ is defined as

$$
\mathbf{A} = \begin{pmatrix} 2 & 0.5 & -0.5 \\ 0.5 & 2.5 & -0.5 \\ -0.5 & -0.5 & 1.5 \end{pmatrix}, \tag{D1}
$$

Improved self-consistency of the Reynolds stress tensor eigenspace perturbation for UQ

with a set of eigenvalues ρ_{i_A} and eigenvectors $\mathbf{v}_{i_A}$.

Tensor $\mathbf{C}$, which is positive semi-definite as well, reads

$$\mathbf{C} = \begin{pmatrix} 1 & 0.5 & 1.5 \\ 0.5 & 2 & 0 \\ 1.5 & 0 & 3 \end{pmatrix}. \tag{D2}$$

The respective set of eigenvalues is ρ_{i_C} and eigenvectors are $\mathbf{v}_{i_C}$.

Tensor $\mathbf{B}$ is constructed using the PCS defined by the eigenvectors of $\mathbf{A}$ and the eigenvalues of $\mathbf{C}$

$$\mathbf{B} = v_{in_A} \begin{pmatrix} \rho_{1_C} & 0 & 0 \\ 0 & \rho_{2_C} & 0 \\ 0 & 0 & \rho_{3_C} \end{pmatrix} v_{jl_A} \approx \begin{pmatrix} 2.19 & 0.55 & -1.11 \\ 0.55 & 3.02 & -0.83 \\ -1.11 & -0.83 & 0.79 \end{pmatrix} \tag{D3}$$

REFERENCES

[1] K. Duraisamy, G. Iaccarino, and H. Xiao, "Turbulence modeling in the age of data," Annual Review of Fluid Mechanics **51**, 357–377 (2019).

[2] H. Xiao and P. Cinnella, "Quantification of model uncertainty in RANS simulations: A review," Progress in Aerospace Sciences **108**, 1–31 (2019).

[3] M. Emory, J. Larsson, and G. Iaccarino, "Modeling of structural uncertainties in Reynolds-averaged Navier-Stokes closures," Physics of Fluids **25**, 110822 (2013).

[4] G. Iaccarino, A. A. Mishra, and S. Ghili, "Eigenspace perturbations for uncertainty estimation of single-point turbulence closures," Physical Review Fluids **2**, 024605 (2017).

[5] N. Razaaly, G. Gori, G. Iaccarino, and P. M. Congedo, "Optimization of an orc supersonic nozzle under epistemic uncertainties due to turbulence models," in *GPPS 2019-Global Power and Propulsion Society* (2019).

[6] A. A. Mishra and G. Iaccarino, "Uncertainty estimation for Reynolds-averaged Navier–Stokes predictions of high-speed aircraft nozzle jets," AIAA Journal **55**, 3999–4004 (2017).

[7] L. W. Cook, A. Mishra, J. Jarrett, K. Willcox, and G. Iaccarino, "Optimization under turbulence model uncertainty for aerospace design," Physics of Fluids **31**, 105111 (2019).

[8] A. A. Mishra, J. Mukhopadhaya, J. Alonso, and G. Iaccarino, "Design exploration and optimization under uncertainty," Physics of Fluids **32**, 085106 (2020).

[9] M. Chu(楚明翰), X. Wu, and D. E. Rival, "Quantification of Reynolds-averaged Navier-Stokes model-form uncertainty in transitional boundary layer and airfoil flows," Physics of Fluids **34** (2022), 10.1063/5.0107547, 107101.

[10] M. Chu(楚明翰), X. Wu, and D. E. Rival, "Model-form uncertainty quantification of Reynolds-averaged Navier-Stokes modeling of flows over a SD7003 airfoil," Physics of Fluids **34** (2022), 10.1063/5.0116282, 117105.

[11] C. García-Sánchez, D. Philips, and C. Gorlé, "Quantifying inflow uncertainties for cfd simulations of the flow in downtown oklahoma city," Building and environment **78**, 118–129 (2014).

[12] G. Lamberti and C. Gorlé, "Uncertainty quantification for RANS predictions of wind loads on buildings," in *Proceedings of the XV Conference of the Italian Association for Wind Engineering* (Springer International Publishing, Cham, 2019) pp. 402–412.

[13] A. Eidi, R. Ghiassi, X. Yang, and M. Abkar, "Model-form uncertainty quantification in RANS simulations of wakes and power losses in wind farms," Renewable Energy **179**, 2212–2223 (2021).

[14] S. D. Hornshøj-Møller, P. D. Nielsen, P. Forooghi, and M. Abkar, "Quantifying structural uncertainties in Reynolds-averaged Navier-Stokes simulations of wind turbine wakes," Renewable Energy **164**, 1550–1558 (2021).

[15] G. Gori, O. Le Maitre, and P. M. Congedo, "A confidence-based aerospace design approach robust to structural turbulence closure uncertainty," Computers & Fluids **246**, 105614 (2022).

[16] J. Heyse, A. A. Mishra, and G. Iaccarino, "Estimating RANS model uncertainty using machine learning," Journal of the Global Power and Propulsion Society , 1–14 (2021).

[17] A. Eidi, N. Zehtabiyan-Rezaie, R. Ghiassi, X. Yang, and M. Abkar, "Data-driven quantification of model-form uncertainty in Reynolds-averaged simulations of wind farms," Physics of Fluids **34** (2022), 10.1063/5.0100076, 085135, https://pubs.aip.org/aip/pof/article-pdf/doi/10.1063/5.0100076/16585042/085135_1_online.pdf.

[18] J. Mukhopadhaya, B. T. Whitehead, J. F. Quindlen, J. J. Alonso, and A. W. Cary, "Multi-fidelity modeling of probabilistic aerodynamic databases for use in aerospace engineering," International Journal for Uncertainty Quantification **10**, 425–447 (2020).

[19] N. Nigam, S. Mohseni, J. Valverde, S. Voronin, J. Mukhopadhaya, and J. J. Alonso, "A toolset for creation of multi-fidelity probabilistic aerodynamic databases," in *AIAA Scitech 2021 Forum* (2021) p. 0466.

[20] W. Edeling, G. Iaccarino, and P. Cinnella, "Data-free and data-driven RANS predictions with quantified uncertainty," Flow Turbulence and Combustion **100**, 593–616 (2018).

[21] C. Gorlé, S. Zeoli, M. Emory, J. Larsson, and G. Iaccarino, "Epistemic uncertainty quantification for Reynolds-averaged Navier-Stokes modeling of separated flows over streamlined surfaces," Physics of Fluids **31**, 035101 (2019), https://doi.org/10.1063/1.5086341.

[22] A. A. Mishra, J. Mukhopadhaya, G. Iaccarino, and J. Alonso, "An uncertainty estimation module for turbulence model predictions in SU2," AIAA Journal **57** (2018), 10.2514/1.J057187.

[23] M. Matha, K. Kucharczyk, and C. Morsbach, "Evaluation of physics constrained data-driven methods for turbulence model uncertainty quantification," Computers & Fluids , 105837 (2023).

[24] W. L. Oberkampf and T. G. Trucano, "Verification and validation in computational fluid dynamics," Progress in aerospace sciences **38**, 209–272 (2002).

[25] F. Stern, R. V. Wilson, H. W. Coleman, and E. G. Paterson, "Comprehensive approach to verification and validation of CFD simulations-part 1: methodology and procedures," J. Fluids Eng. **123**, 793–802 (2001).

[26] A. A. Mishra and G. Iaccarino, "Theoretical analysis of tensor perturbations for uncertainty quantification of reynolds averaged and subgrid scale closures," Physics of Fluids **31**, 075101 (2019).

[27] P. J. Roache, *Verification and validation in computational science and engineering*, Vol. 895 (Hermosa Albuquerque, NM, 1998).

[28] AIAA CFD Committee, "Guide: Guide for the verification and validation of computational fluid dynamics simulations (AIAA G-077-1998 (2002))," (1998).

[29] J. L. Lumley and G. R. Newman, "The return to isotropy of homogeneous turbulence," Journal of Fluid Mechanics **82**, 161–178 (1977).

[30] U. Schumann, "Realizability of Reynolds-stress turbulence models," The Physics of Fluids **20**, 721–725 (1977), https://aip.scitation.org/doi/pdf/10.1063/1.861942.

[31] L. Terentiev, *The Turbulence Closure Model Based on Linear Anisotropy Invariant Analysis*, Ph.D. thesis, Friedrich-Alexander-Universität Erlangen-Nürnberg (FAU) (2006).

[32] S. Banerjee, R. Krahl, F. Durst, and C. Zenger, "Presentation of anisotropy properties of turbulence, invariants versus eigenvalue approaches," Journal of Turbulence **8**, N32 (2007).

[33] C. G. Speziale, "Analytical methods for the development of Reynolds-Stress closures in turbulence," Annual Review of Fluid Mechanics **23**, 107–157 (1991).

[34] G. Mompean, S. Gavrilakis, L. Machiels, and M. Deville, "On predicting the turbulence-induced secondary flows using nonlinear k-ε models," Physics of Fluids **8**, 1856–1868 (1996).

[35] T. Craft, B. Launder, and K. Suga, "Development and application of a cubic eddy-viscosity model of turbulence," International Journal of Heat and Fluid Flow **17**, 108–115 (1996).

[36] F. Lien and M. Leschziner, "Assessment of turbulence-transport models including non-linear rng eddy-viscosity formulation and second-moment closure for flow over a backward-facing step," Computers & Fluids **23**, 983–1004 (1994).

[37] J. B. Lasserre, "A trace inequality for matrix product," IEEE Trans. Automatic Control **40** (1995).

[38] K.-S. Choi and J. L. Lumley, "The return to isotropy of homogeneous turbulence," Journal of Fluid Mechanics **436**, 59–84 (2001).

[39] F. Menter, M. Kuntz, and R. Langtry, "Ten years of industrial experience with the SST turbulence model," Turbulence, Heat and Mass Transfer **4**, 625 – 632 (2003).

[40] M. Lee and R. D. Moser, "Direct numerical simulation of turbulent channel flow up to $Re_\tau \approx$ 5200," Journal of Fluid Mechanics **774**, 395–415 (2015).